Tectonophysics 766 (2019) 194–204

Contents lists available at ScienceDirect

Tectonophysics

journal homepage: www.elsevier.com/locate/tecto

Far-field strain transmission and contractional step-overs

Ioan Munteanu[b,*], E. Willingshofer[a], L. Matenco[a], D. Sokoutis[a,c], C. Dinu[d], S. Cloetingh[a]

[a] Utrecht University, Department of Earth Sciences, Princetonlaan 4, 3584B Utrecht, the Netherlands
[b] Repsol Exploration, UK Exploration Team, Mendez Alvaro 44, 28045 Madrid, Spain
[c] Department of Geosciences, University of Oslo, PO Box 1047, Blindern, N-0316 Oslo, Norway
[d] University of Bucharest, Faculty of Geology and Geophysics, Traian Vuia 6, 020956 Bucharest, Romania

ARTICLE INFO

Keywords:
Far field strain transmission
Contractional step-overs
Analogue modelling
Lateral rheology variation
Transfer zone
Deformation
Black Sea
Makran

ABSTRACT

In contractional (subduction/collisional) settings, convergence is accommodated by the formation of thin- and thick-skinned thrust and fold belts. The transmission of such deformation over larger distances into orogenic foreland areas is influenced by the inherited rheological characteristics of continental lithosphere. Lateral rheological variations parallel to the strike of continental foreland areas creates contrasting geometries and sequences of deformation that interact during orogenic build-up. We investigate the far-field transmission of strain within a continental lithosphere characterized by a laterally variable rheology through physical analogue modelling. Rheological weak crustal zones were introduced at distance from an advancing backstop to study the progressive along strike linkage and interference of structures during contraction. The results reveal that rheologically weak crustal zones localise far-field contractional deformation. When the size of weak zones, by means of their horizontal extend to depth ratio, is large, deformation localises at the boundaries of the weak zone where they lead to the formation of large-offset faults. Subsequently the faults migrate along-strike into areas that are rheologically stronger. When the size of the weak zone is reduced, a large-scale contractional step-over forms in orogenic forelands, where rheologically contrasting domains transmit out-of-sequence deformation by a gradual migration of thrust offsets and fold amplitudes along their strike. These results show that crustal scale orogenic step-overs do not always reflect variations in the geometry of the plate boundary (indenter) or along-strike gradients in shortening rates. Such features may also form in response to variations in rheology, as the ones created by inherited extensional basins situated at large distances from plate boundaries in the orogenic foreland.

1. Introduction

The continental lithosphere is characterized by large lateral variations in rheological properties (e.g., Tesauro et al., 2012; Watts, 2001) that have a significant influence on regional stress field and, therefore, on the transmission and localisation of deformation (Baes et al., 2011; De Franco et al., 2008). Rheological variations are often controlled by inherited features stemming from older deformation phases, which control the structural grain, juxtapose units of different composition or lead to thermal perturbations (e.g., Burov and Cloetingh, 2009; Doglioni et al., 2007; Erdős et al., 2014; Lacombe and Bellahsen, 2016; Vogt et al., 2017). For example, the formation of extensional basins has a profound impact on the rheological stratification of the lithosphere through the creation of pronounced thermal anomalies, leading to a significant decrease in the integrated strength at short times after the cessation of rapid mechanical extension, or its overall increase at longer time scales (e.g., Cloetingh et al., 2003 and references therein). In the first case, the weakened crust and mantle lithosphere may transmit subsequent contractional deformation at large distances by reducing the brittle/ductile coupling effect (e.g., Smit et al., 2003). Both analogue and numerical modelling studies have investigated the effects of such extensional weak zones on strain localization and the evolution of contractional deformation geometries, particularly focusing on the inversion of graben geometries, the mechanical coupling between layers and domains of different strength and the balance between the amounts of deformation during extension and subsequent contraction (e.g., Brun and Nalpas, 1996; Buiter et al., 2009; Calignano et al., 2015a; Calignano et al., 2017; Dubois et al., 2002; Erdős et al., 2014; Munteanu et al., 2013; Panien et al., 2005; Smit et al., 2003; Sokoutis and Willingshofer, 2011; Willingshofer and Sokoutis, 2009). Upon contraction, deformation can localise at far distances from plate boundaries leading to significant shortening within continental plates or other

* Corresponding author.
E-mail address: ioan.munteanu@repsol.com (I. Munteanu).

https://doi.org/10.1016/j.tecto.2019.06.012
Received 24 January 2019; Received in revised form 9 June 2019; Accepted 15 June 2019
Available online 18 June 2019

orogenic foreland areas, such as observed in the Makran, the Black Sea, Albanides-Dinaridic-Hellenic system, Sierras Pampeanas, and other areas (e.g. Lacombe and Bellahsen, 2016; Roure, 2008; Ziegler et al., 2002; Ziegler et al., 1998). Physical analogue modelling studies have revealed the effectiveness of strain transmission at large distances from the active deformation area as a function of the inherited crustal or lithospheric rheology that focuses contraction at boundaries between rheological weak and strong areas (Calignano et al., 2017; Del Ventisette et al., 2006; Dombrádi et al., 2010; Willingshofer and Sokoutis, 2009), or at terminations of decoupling horizons (e.g., Cotton and Koyi, 2000; Luth et al., 2010; Smit et al., 2003). These studies invoked across-strike alternations between weak and strong domains as often observed in orogens and their forelands (e.g., Banks et al., 1997; Cotton and Koyi, 2000; Doglioni et al., 2007; Tarapoanca, 2004). In contrast, along-strike rheological changes at distance to the orogenic hinterland and their influence on strain localisation and subsequent propagation of deformation is not understood. In particular, we seek to gain insight in how inherited weak zones in orogenic forelands control the transmission of strain over large distances, the sequence and orientation of evolving structures as well as their along strike propagation across orogen-parallel strength variations. We use physical analogue modelling to document the structural and kinematic characteristics of transfer zones that connect domains of different strength within the continental crust.

2. Modelling strategy

A series of lithospheric-scale physical analogue experiments has been performed at the Tectonic Laboratory (TecLab) at Utrecht University to investigate far-field strain transmission during compression (Fig. 1 and Tables 1 and 2). The models consist of two mechanically different crustal domains referred to as brittle-ductile (BDD) and brittle domains (BD), respectively (Figs. 1–3), which are floored by the same ductile upper lithospheric mantle (DLM). Different from a reference model type 1, all other models contain "inherited" crustal weak zones within the brittle-ductile domain, incorporated by introducing one or more ductile layers, with variable thickness and geometries at the base of the brittle crust (Fig. 1 and Table 2). These zones of weakness with finite lateral extent introduce across and along-strike rheological changes, which represent inherited structures, such as extensional grabens with variable thickness and geometries. The "size" of the weak zone, expressed here by the ratio between brittle upper crustal thickness and the weak zone width, defines the weakness ratio (Fig. 1), a parameter that has an important effect in the final geometry of our models (WR, Table 2).

We use the lateral extent-to-depth ratio ("size") as a proxy of the rheological impact of the weak zones (WZ_w/h_{bc}, Fig. 1, Table 2). Shortening was achieved by moving one of the confining walls at a constant rate of 2 cm/h in a direction parallel to the BD-BDD boundary and orthogonal to the strike of the weak zones (Fig. 1 and Table 2). The total applied shortening was 5 cm in all models, which represents 8% of the entire model (2.5 cm at 50% stage, representing 4% of the entire model). This value is comparable with the observations in our discussed natural scenarios, such as the 30-32 km (6–7%) minimum amount of shortening calculated for the Black Sea system (Munteanu et al., 2011; Stuart et al., 2011). We were not able to find shortening values for the Afgan and Lut blocks, however in the case of Zagros Mountains the total shortening is about 57–85 km, which might represent an acceptable proxy (Hatzfeld et al., 2010, which is about 10% of the entire system). The moving wall had the same height as the experimental box and slightly smaller in length, allowing the asthenospheric fluid to flow behind it. The experiments were performed under normal gravity conditions. Friction along sidewalls was reduced by using fixed thin glass plates along the long side of the tank. The effectiveness of this measure is demonstrated by the grid lines that show almost no dragging effect at their margin and terminate perpendicular to the sidewalls, as well as by the fact that structures do not nucleate at the sidewalls, but inside the models. In agreement with other modelling studies (e.g. Calassou et al., 1993; Koyi and Sans, 2006; Farzipour-Saein and Koyi, 2014; or Calignano et al., 2017), these observations show that the curvature of structures in our models is an expression of lateral rheological changes rather than a boundary effect. The models were allowed to re-equilibrate isostatically for a time period of 20 h. The deformation was monitored through top-view imaging and laser scanning at constant intervals. The final geometry was also analysed through studying regular spaced cross-sections, obtained by cutting the model parallel to the convergence directions after its wetting and freezing. The loading effect of water and sand used to coat and preserve structures was removed through restoring the cross-sections topography to the elevation acquired at the last stage of deformation by using the laser scanning

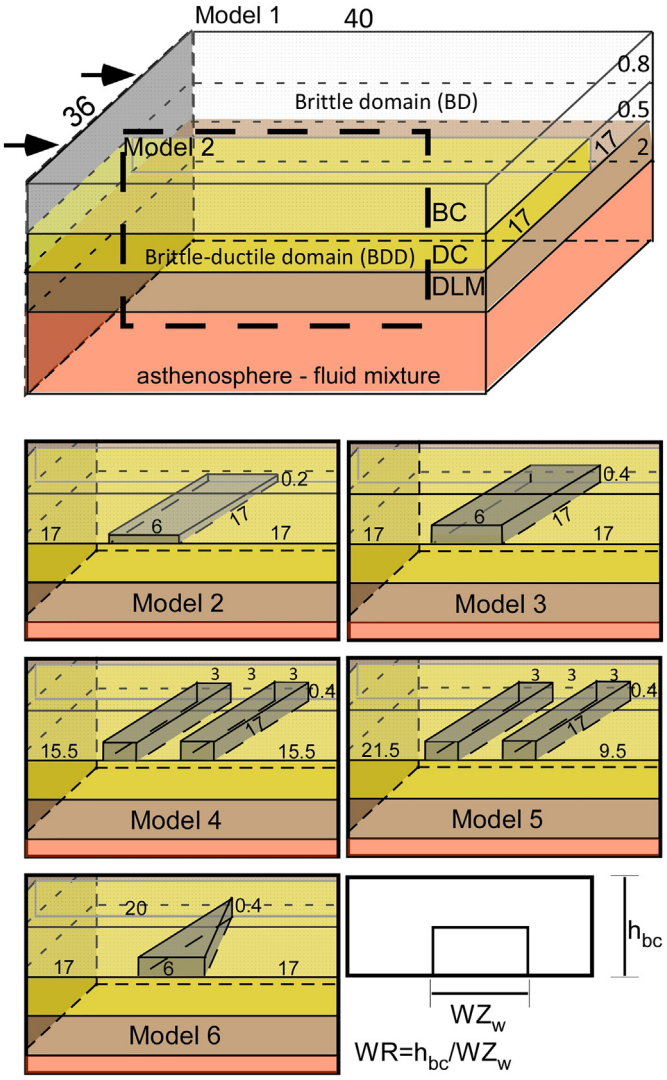

Fig. 1. Sketch illustrating the analogue modelling setup. The model simulates a continental lithosphere composed of two (brittle crust over ductile mantle in the brittle domain (BD)) and three (brittle crust over ductile crust and ductile mantle lithosphere, (BDD)) layers. Note that Model 1 is uniform in the brittle and brittle-ductile domains, i.e. no weak zone. Models 2–6 have a variable geometry of the weak zone in the brittle-ductile domain. The sketch in the lower right corner, illustrates the way how we calculate the weaknesses ration (WR) parameter in Table 2. The black arrows indicate the direction of contraction. BC — brittle crust; DC — ductile crust, DLM ductile lithospheric mantle, h_{bc} — brittle crust thickness, WZ_W — weak zone width. The small numbers are illustrating the models and layers dimensions in cm (see also Table 2).

Table 1
Summary of the model parameters and their natural equivalents. The coefficient of friction has been measured with a ring shear tester at GFZ Potsdam (for details see Willingshofer et al., 2018). The effective viscosity of the silicone mixtures has been determined with a Coni-cylindrical viscometer under room temperature (21 ± 1 °C).

Materials/parameters		Model	Nature
Upper crust (K-feldspar sand)	Thickness (m)	0.008–0.013 cm	16,000–26,000
	Density (kgm^{-3})	1300	~2600
	Coefficient of internal friction	0.6–0.7	0.75
	Cohesion (Pa)	15–35	6×10^7
Lower crust (silicone mixture)	Thickness (m)	0–0.005	0–10,000
	Density (kgm^{-3})	1400	~2900
	Viscosity (Pas)	1.3×10^4	$\sim 1.25 \times 10^{22}$
	n-value	1.3	3
	Material constant A	7×10^{-6}	
Upper mantle (silicone mixture)	Thickness (m)	0.02	40,000
	Density (kgm^{-3})	1480	3300
	Viscosity (Pas)	1.4×10^4	$\sim 1.5 \times 10^{22}$
	n-value	1.5	4
	Material constant A	2×10^{-6}	
Asthenosphere (Sodium polytungstate and glycerol mixture)	Density (kgm^{-3})	1600	3300
	Viscosity (Pas)	1.2	$\sim 1 \times 10^{19}$
Length of box		40 cm	800 km
Width of box		36 cm	720 km
Shortening rate		2 cm/h	1.5 km/My
Total Shortening		5 cm	100 km
Smoluchowski number (Sm)		4.28–5.65	4.8
Ramberg number ductile crust (*Rm*)		5	6
Ramberg number ductile mantle lithosphere (*Rm*)		75	73
Reynolds number ductile crust (*Re*)		2.9×10^{-9}	1.4×10^{-25}
Reynolds number ductile mantle lithosphere (*Re*)		1.2×10^{-8}	4.2×10^{-25}

DEM. This correction is important for obtaining the deformed geometry of the mantle lithosphere.

2.1. Materials and Scaling

In our experiments, dry feldspar sand with a grain size of 0.1–0.3 mm, density of 1300kgm^{-3}, coefficient of internal friction of 0.4 (dynamic) to 0.7 (static) and cohesion of 15–35 Pa (Willingshofer et al., 2018) represents the brittle layer. The ductile layers in the system consist of mixtures of Rhodorsil gum-type silicone and Barium sulphate similar to the experiments described in Willingshofer and Sokoutis (2009). Their viscosities (see Table 1) scale to lower crust and upper mantle viscosities in the order of 1.25 and 1.5*10^{22} Pas, respectively. Such lower crust and upper mantle viscosities are in agreement with lithospheric strength profiles where the peak strength resides in the brittle crust (eg. Burov and Toussaint, 2007 and references therein). The weak zone(s) are made of the same ductile material as ductile crust. The whole model floated on a low viscosity, high-density fluid made of a sodium polytungstate and glycerol mixture that simulated the asthenosphere (Fig. 1 and Table 1).

Scaling is based on the principles of geometrical, rheological, dynamical, and kinematic similarity (Hubbert, 1937; Ramberg, 1981; Sokoutis et al., 2000; Weijermars and Schmeling, 1986), using dimensionless ratios of gravitational to brittle strength (cohesion) and viscous forces (Table 1). To achieve dynamic similarity these ratios, expressed in the Ramberg number (*Rm*) for ductile layers, must be the same for the model and the natural prototype (Table 1):

$$Rm = \rho_d g h_d / \eta \dot{\varepsilon} = \rho_d g h^2{}_d / \eta v \quad (1)$$

where ρ_d and h_d are respectively the density and thickness of the ductile layer, g is the acceleration due to gravity (g = 9.81 m/s^2), η is the effective viscosity and $\dot{\varepsilon}$ is the strain rate given by the ratio between the mean velocity of convergence, v, and the thickness of the ductile layer h_d. Similarly, we used the Smoluchowski number (Sm) defined by Ramberg (1981) for scaling brittle deformation, by considering the ratio between gravitational and frictional forces:

$$Sm = \rho_b g h_b / c + \mu_b \rho_b g h_b \quad (2)$$

where ρ_b, g, h_b, c and μ_b are respectively the density, acceleration due to gravity, thickness, cohesive strength, coefficient of intern friction of the brittle layer (Table 1).

The dynamic similarity requires that other non-dimensional numbers involving inertial forces are equivalent in model and nature, such as for the Reynolds number, *Re* (ratio of inertial forces to viscous forces) (Dombrádi et al., 2010; Ramberg, 1981):

$$Re = \rho v l / \eta \quad (3)$$

where ρ stands for the density, v is the velocity of convergence, l is the length and η is the viscosity.

Convergence rates are averaged over the duration of the experiments and are scaled to nature to represent slowly converging systems with convergence rates of a few millimetres per year (Table 1).

Table 2
Geometrical parameters used in the analogue modelling. Where h_{dml} - thickness of ductile lithospheric mantle, h_{dc} - thickness of the ductile crust, h_{bc} - thickness of the brittle crust, WZ - weak zone, WZw - weak zone width.

Model	Total thickness (cm)	h_{dml} (cm)	h_{dc} (cm)	h_{bc} (cm)	WZ number	Weakness ratio (WZ_w/h_{bc})	WZ geometry (L × W × H) (cm)	WZ position (cm)
1	3.3	2	0/0.5	0.8/1.3	0			
2	3.3	2	0/0.5	0.8/1.3	1	7.50	17 × 6 × 0.4	17
3	3.3	2	0/0.5	0.8/1.3	1	7.50	17 × 6 × 0.2	17
4	3.3	2	0/0.5	0.8/1.3	2	3.75	17 × 3 × 0.4	15.5/21.5
5	3.3	2	0/0.5	0.8/1.3	2	3.75	17 × 3 × 0.4	18.5/24.5
6	3.3	2	0/0.5	0.8/1.3	1	7.50	17 × 6/0.1 × 0.4	14 to 20

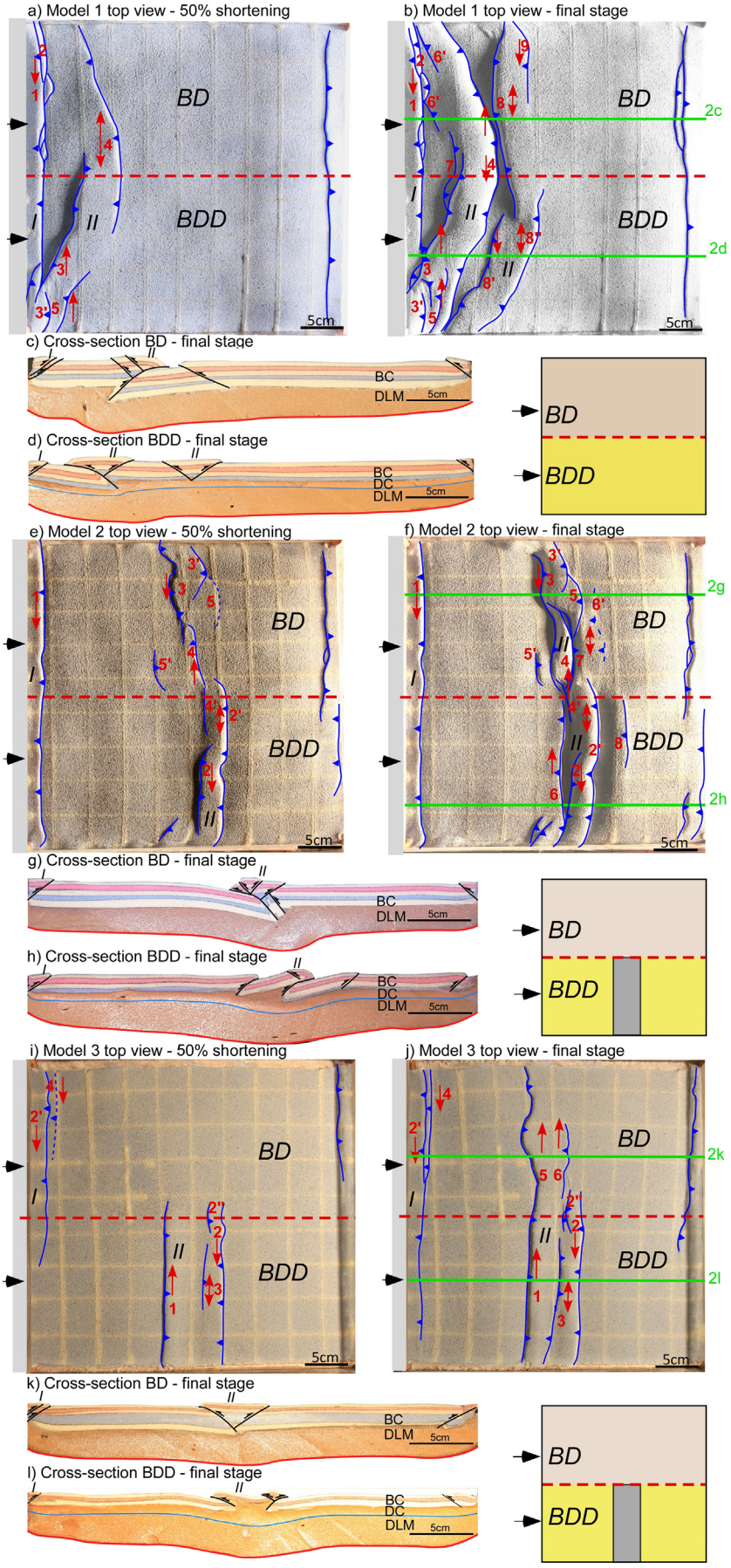

Fig. 2. Modelling results for models type 1–3. a, e, i) Structural interpretation of the top-view of the model displayed at 50% shortening and b, f, j) at the end of shortening. Black thick arrows represent the direction of shortening, as imposed by the moving wall. The red arabic numbers represent the sequence of deformation structures. The red arrows indicate the direction of lateral deformation migration. Green continuous lines are the traces of cross-sections in panels c, d, g, h, k, l, through the model at final stage of deformation. Note the differentiation between the various lithospheric layers by a red thick discontinuous line. Italic black colour roman letters represent set I and II contractional structures. Inset, top view of the modelling setup. Further conventions as in Fig. 1. (For interpretation of the references to colour in this figure legend, the reader is referred to the web version of this article.)

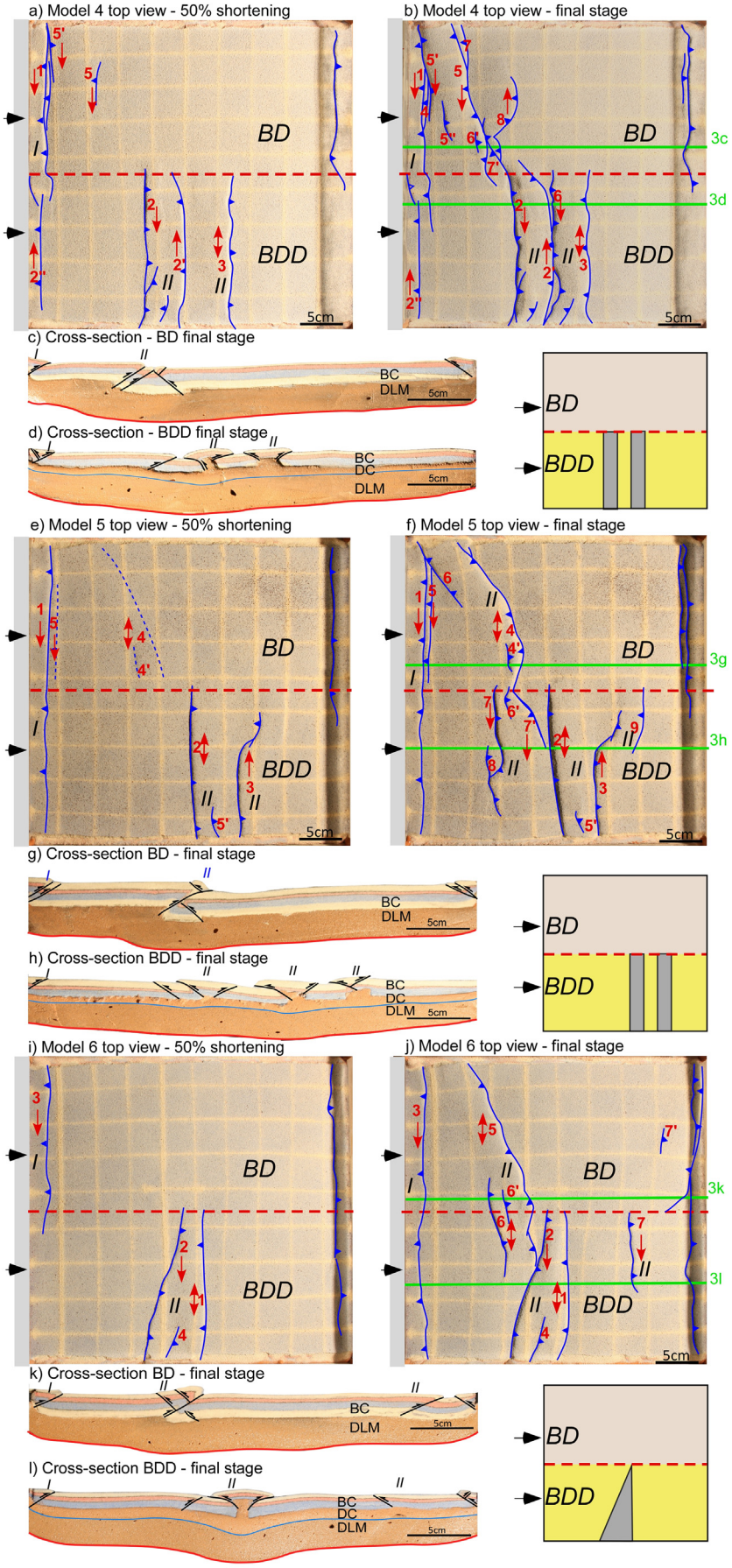

Fig. 3. Modelling results for models type 4–6. a, e, i) Structural interpretation of the top-view of the model displayed at 50% shortening and b, f, j) at the end of shortening. Black thick arrows represent the direction of shortening, as imposed by the moving wall. Red arabic numbers represent the sequence of deformation structures. The red arrows indicate the direction of lateral deformation migration. Green continuous lines are the traces of cross-sections in Fig. 2 c, d, g, h, k, l through the model at final stage of deformation. Note the differentiation between the various lithospheric layers by a red thick discontinuous line. Italic roman letters represent set I and II contractional structures. Inset, top view of the modelling setup. (For interpretation of the references to colour in this figure legend, the reader is referred to the web version of this article.)

Viscosity depends on strain rate and, therefore, on the rate of convergence. Consequently, we have chosen the experimental convergence rate in such a way to ensure dynamic similarity with respect to the natural prototype as expressed in the Ramberg number (Table 1). The shortening velocity and other modelling parameters are shown in Table 1. The experiments were built with a length scale factor of $5 * 10^{-5}$, which means that 1 cm in the model corresponds to 20 km in nature (see, Brun and Nalpas, 1996; Michon and Sokoutis, 2005).

2.2. Analogue modelling simplification and limitations

While analogue modelling is a tool for studying first order characteristics of natural processes, they cannot accurately reproduce their complexity. However, proper scaling, carefully implemented simplification together with a detailed characterization of the material properties results in appropriate understanding of large-scale tectonic processes that are relevant for the natural prototype. We are aware that factors such as temperature variations with depth or sediment transfer, eroded from structural heights and deposited in newly formed basins may modify strength profiles and influence the localisation of deformation (e.g., Ranalli and Murphy, 1987; Burov and Toussaint, 2007). These factors are, however, less important in context of our study as we assume that the lateral crustal strength variations reside within a thermally equilibrated lithosphere and that the amount of topography and thus erosion, created through the inversion of inherited rift structures is modest.

Building the model within a tank inherently may lead to small heterogeneities at the backwall, such as thickness variations of the ductile or brittle layers. As a consequence, we refrained from interpreting structures that developed early in the model evolution at the backwall, because they might be related to such small heterogeneities; yet in most cases they are probably an expression of strain transmission.

3. Modelling results

The modelling results are illustrated using interpreted final stage top horizontal views and cross-sections, one for each domain (BD and BDD, Figs. 2 and 3). The sequence of deformation is indicated by consecutive numbering of structures whereas the propagation direction is illustrated by arrows (Figs. 2 and 3). Note that although we have drawn the structures formed at the opposite side of the indenter, these are considered boundary effects and, therefore, are not included in interpretation.

3.1. Deformation pattern

The first order features observed in all models are the presence of two spatially separated structural systems, consisting of thrust faults and/or folds (Figs. 2a, b, e, f, i, j and 3a, b, e, f, i, j). The structures that form in the immediate vicinity of the advancing backstop, labelled as set I in Figs. 2 and 3, are the first ones to form in the brittle domain and in the brittle-ductile domain when it is devoid of strength variations (model type 1, Fig. 2a and c) or when the distance to the weak zone within the brittle-ductile domain is small and the weak zone is narrow (model type 4, Figs. 3a–c and 4). In the reference model (e.g. without weak zone, type 1) a set II structures form in close proximity with the first one, in a foreland breaking sequence (Fig. 2a). In contrast, in models where weak zones have been incorporated, the second set of structures (II in Figs. 2 and 3) forms at far distances from the backstop and always initiates above the weak zone(s) from where it propagates laterally along strike. The propagation direction differs from model to model, inward (towards BD/BDD boundary) in model type 1 (structure 3, Fig. 2a) and type 3 (structure 1, Fig. 2e); outward in model type 2 (structure 2 in Fig. 2e) and type 4 (structure 2 Fig. 3a), divergent in model type 5 (structure 2 in Fig. 3e) and type 6 (structure 1 in Fig. 3i). There is a general forward propagation sequence in almost all of the models, with the formation of set I structures and then set II. The exceptions are model type 6 and in part 5 where the deformation propagates dominantly backwards with the first structure localized at the weak zone (Figs. 3e, i and 4). These set II result from far-field transmission of deformation (Fig. 4) and are observed in all models that contain weak zones, either distributed in the entire model or restricted to the brittle-ductile domain (Figs. 2 and 3). The presence of the weak zone localises deformation at the contact between the ductile layer and the neighbouring brittle domain by the formation of thrust faults and associated ramp anticlines (Figs. 2g, h, k and l, 3g, h, k and l). The movement along a lower crustal, layer parallel, shear zone is accommodated by accumulating ductile material in detachment folds and the formation of large-scale pop-up structures (Fig. 2g). Foreland directed thrusting with large offset faults (more than 50% of brittle layer thickness) is favoured for models containing one thin weak zone (model type 2, Fig. 2f, g and h), whereas the presence of thicker weak zones (models type 3–6) dominantly leads to a pop-up style of deformation (e.g. Figs. 2j, k, l and 3d, h and i). Whenever far-field deformation is observed, shortening along set I structures is reduced in both brittle and brittle-ductile domains, while set II structures accommodate most shortening (Fig. 4).

A large-scale transfer zone formed at the BD/BDD contact, is observed in models that focus deformation near the indenter in the brittle domain and far-field transmission of strain is recorded in the brittle-ductile domain. Such models are the ones where the width of the weak zone is narrowing towards the brittle domain (models type 6, Fig. 3i and j), or where multiple, narrow weak zones are separated by stronger domains (models type 4 and 5, Fig. 3b, f and j). This transfer zone records a swing in structural geometries from parallel with the indenter to oblique near the contact between the brittle and brittle-ductile domains. Forethrusts and backthrusts within the brittle-ductile domain and specifically at the location of the weak zones, form early in the deformation history (see top-view images at 50% bulk shortening, Fig. 3a, b and i) and terminate against the brittle domain or are connected to oblique forethrusts within the brittle domain. In the latter case thrust structures with opposite vergence are linked (e.g. in model type 4, backthrust 2 within the brittle-ductile domain is linked to forethrust 5 within the brittle domain; Fig. 3b). Thrusts that terminate at the transition between brittle and brittle-ductile domains define a sinistral step-over (Fig. 3b, f and j), created by the differential motion between the brittle domain concentrating the deformation near the indenter and the brittle-ductile domain transmitting far-field strain (Fig. 3). The overall geometry of this transfer zone in cross-sections is dominated by high-angle forethrusts that are locally associated with low-offset backthrusts (Fig. 3k). The geometry of the transfer zone is conditioned by the width of the weak zone in the brittle-ductile domain (see also Table 2). When this width is small (weakness ratio 3.75) the transfer zone is narrow and the transition sharp (Fig. 3f). When the width increases (weakness ratio 7.5), such as in models with one laterally variable weak zone or multiple zones separated by stronger domains (models type 4–6, Fig. 1), the transfer zone is wide and consists of structures that initiate and propagated from the brittle domain towards the brittle ductile domain (compare the top-views at 50% and final stage of deformation, Fig. 3a with b, e with f and i with j).

3.2. The effects of rheological weak zones at crustal level

All models that contain lateral strength variations within the brittle-ductile domain show that deformation localises at the boundary between weaker and stronger crust. The width of the weak zone in the brittle-ductile domain affects the lateral transmission of far-field deformation in the brittle domain. When this width is large (weakness ratio 7.5, Table 2), the early formation of far-field structures in the brittle-ductile domain (15–20% of bulk shortening, Fig. 4) controls the subsequent initiation of deformation along strike in the brittle domain by a gradual lateral increase in offset (Figs. 2e, f, j and 3b, e, f and j).

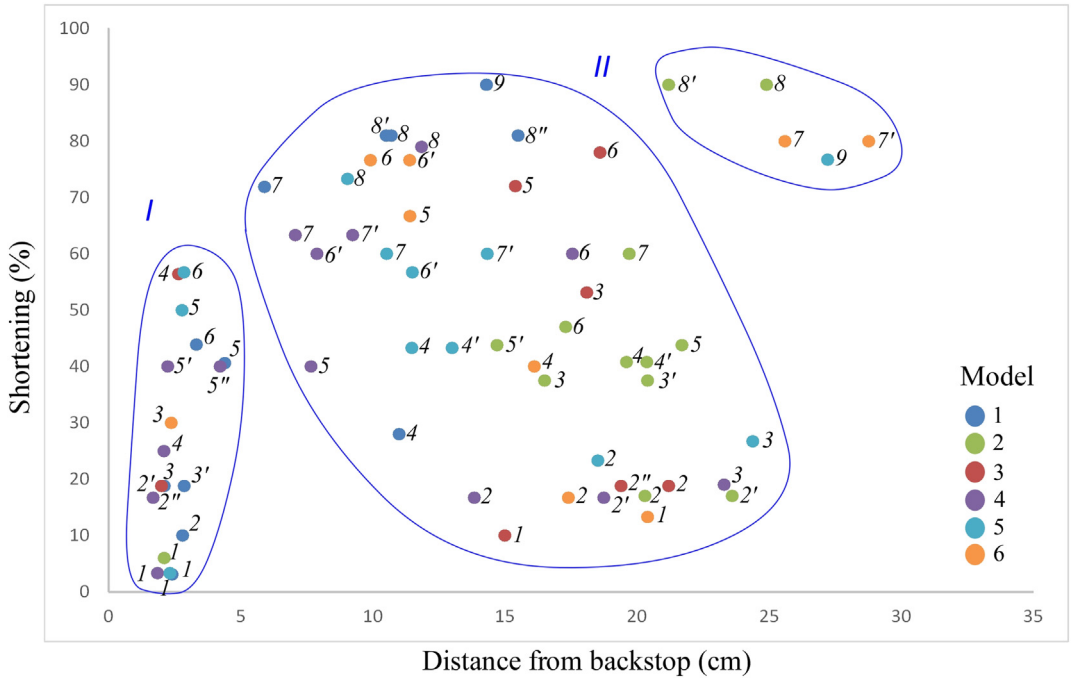

Fig. 4. Graph showing localization of the deformation as a function of shortening versus distance from the backstop. Deformation sequence is represented by numbers. Note the 3 main groups, one belonging to the set I and two to the set II contractional structures. The most effective in far-field strain transmission are models 3, 5 and 6 with structures formed during later stages at large distance from the indenter. All of these models have in common the inherited large distance between indenter and weak zone location. A shorter distance between them is not favorable for far-field strain transmission.

This along-strike migration of far-field deformation into the brittle domain localises thrusting and imposes the formation of new structures that migrate backwards into brittle-ductile domain (models type 2 and 6, Figs. 2f and 3j). Similar kinematic sequences migrating from the brittle-ductile into the brittle domains and backwards are also observed in models with a transfer zone connecting the set I and set II structures (Fig. 2c, d and g). When the type I structures migrate laterally along strike into the brittle-ductile domain, the transfer zone has a symmetric pop-up geometry (Fig. 2j and l). If the weak zone is narrow, such as in models 4–6, the obliqueness of thrust structures extents across the entire width of the strong domain, irrespective of the initial distance between the moving wall and the weak zone (compare models 4 and 5, Figs. 1 and 3). This contrasts with models that have a wide weak zone initially (models 2 and 3, Figs. 1 and 2). In these cases, deformation initiates at the boundaries of the weak zones, but propagates along-strike into the strong domains (BD) maintaining the overall orientation of structures, ie. striking orthogonal to the shortening direction. These differences in orientation are probably related to a combination of where shortening is accommodated and the displacement on individual thrusts. In all cases where one or multiple weak zones are present, deformation localises at the boundaries of the weak zones and initially develops independently of structures in the brittle domain, which typically start close to the moving wall (Fig. 4). These initially independent areas of deformation aim at connecting to maintain kinematic compatibility through hard linkage as in model 4 or through the development of zones of overlap (models type 5 and 6, Fig. 3). Additionally, large offset thrusts seem to favour along-strike fault growth across domains of different rheology (e.g. model type 3) whereas low offset faults (less than 25% brittle crust thickness) terminate against the stronger domain (models 4–6). As the rheology difference is related to a lateral increase in brittle layer thickness, it emerges that the work needed for the faults to propagate into domains with higher normal stress is insufficient for low slip faults (Herbert et al., 2015).

The overall lateral strain transmission affects significantly the sequence of deformation. In models where the weak zone is not present (uniform distribution both in the brittle and brittle-ductile domains), deformation starts near the indenter and gradually propagates farther into the model. When a weak zone is present, the lateral strain transmission from the brittle-ductile towards the brittle domains and backwards induces significant out-of-sequence thrusting as indicated in Fig. 4 by decreasing distance between the moving wall and newly formed structures. The backward migration from the BD into BDD is more evident in models 5 and 6. It occurs after the formation of transfer zone (Fig. 3e and j), with the formation of new structures behind the weak zone, closer to the indenter (structure 6 and 7 in type 5 models, Fig. 3f; structures 6 and 6′ in models type 6, Fig. 3j). The overall pattern remains a foreland-breaking sequence, with the youngest structures 7 and 9 formed further away from the weak zone (Fig. 3f and j); yet in more detail we also observed oscillations between forward and out of sequence thrusting, during the lateral migration (Figs. 2f, j and 3b, f, and j).

3.3. The effects of rheological weak zones at lithospheric level

Due to its prevailing ductile behaviour, shortening is dominantly accommodated in the lithospheric mantle by folding, which can be best observed by analysing the geometry at the base of the lithosphere (base of DLM cross-section in Figs. 2 and 3). In models with no weak zone (model type 1), this base of the lithosphere is asymmetrically folded in both domains (Fig. 2c, d) with the asymmetry being controlled by the faults with the largest offset in the crust. In contrast, the mantle layer is folded symmetrically were a weak zone is present (models type 2–6), with a maximum amplitude located below the type II crustal structures (Figs. 2g, h, k, l and 3c, d, g, h, k, l). The fold amplitude correlates with the width of the weak zone and is larger in the models with one large weak zone (type 2, 3 and 6, Figs. 2g,h, k, l and 3k, l) when compared with models with 2 separated weak zones (type 4 and 5, Fig. 3c, d, g and h). In other words, a larger amount of deformation localization at crustal weak zone will create larger lithospheric mantle folds. In contrast, a low amount of deformation localization at crustal weak zones, or distributed across multiple structures, is accommodated by broad, low amplitude lithospheric mantle folds (models type 4 and 5, Fig. 3c,

d, g and h). Hence, deformation of the upper lithospheric mantle (DLM, Figs. 1–3) is controlled by the localisation of deformation in the crust.

The weak zone thickness does not seem to have a significant influence over the folding amplitude of the lithospheric mantle in the brittle-ductile domain, as observed by comparing the cross-sections in Fig. 2h and l and VI (model type 2 and 3 respectively). However, it does influence the amplitude and symmetry of the lithospheric mantle folding in the brittle domain, where a large, almost symmetric fold can be observed in models with a thicker and larger weak zone (type 3, Fig. 2k).

4. Possible inferences for natural analogues

4.1. Strain localization and rheological heterogeneities in the crust, inferences from previous and current analogues modelling

Far-field transmission of contractional deformation is rather common in intra-plate settings, including orogenic forelands, facilitated by the presence of rheological heterogeneities in the crust and/or mantle lithosphere. This is commonly interpreted in the context of inherited extensional grabens, such as the Makran contractional wedge (McCall and Kidd, 1982; Burg, 2018), or in variable distribution of ductile salt layers, such as the Potwar Basin of Pakistan (Cotton and Koyi, 2000; Smit et al., 2003), the southern Pyrenees (Koyi and Sans, 2006), the Western Black Sea (Munteanu et al., 2013) and along the Albanides at the transition between the Dinarides and Helenic Orogens (Roure et al., 2010; Vilasi et al., 2009). However, their control on localizing contractional deformation and geometry of the resulting orogen is rather poorly known outside the area where such structures are observed. Our analogue modelling shows a number of key features related to strain transmission across and along the strike of orogenic forelands in the presence of a weakness zone. When such a zone exists in orogenic forelands, it will favour the localization of strain at larger distances from the orogenic front (Fig. 4, set II structures). Interestingly, our models shows this deformation is not restricted to the area where the weak zone is present, but it will migrate laterally along its strike into rheologically stronger domains. These latter domains do not have inherited mechanical weaknesses and, therefore, a localisation of strain near the backstop would be expected, as seen in model type 1 (Fig. 4), defining a foreland-breaking sequence of thrusting, similar to what has been described in Willingshofer et al. (2013) for conditions of strong decoupling of the brittle crust from the underlying layers at the level of the brittle-ductile transition or the Moho.

Detecting the cause of the far-field transmission in these uniform areas may be difficult if the neighbouring weakness zones are not obvious. In such situations, the out-of-sequence character of thrusting provides discriminatory evidences that a weakness zone may be present along the orogenic strike. In this case, out-of-sequence thrusting cannot be attributed to wedge-dynamics at various scales (Morley, 1988; Nieuwland et al., 2000; Graveleau et al., 2012 and references therein), but is solely a consequence of mechanical inheritance. In fact, the strong domain itself acts as new indenter into the weak domain if strain is localized at their contact, transmitting further deformation, as inferred in previous modelling studies (Sokoutis et al., 2005). This behaviour is consistent with results of lithosphere (Calignano et al., 2015a, 2015b; Calignano et al., 2017; Willingshofer et al., 2005; Willingshofer and Sokoutis, 2009; Sokoutis and Willingshofer, 2011) or crustal-scale analogue modelling studies invoking rheological heterogeneities within the crust (e.g. Munteanu et al., 2013, 2014; Nalpas et al., 1995; Sadeghi et al., 2016). We have shown that forward and backward alternation in localization of deformation during the lateral migration between the brittle and brittle-ductile domains is genetically linked to rheological inheritance of weak zones. In contrast, the backward migration from the BD to the BDD domain is controlled by wedge-dynamics, with structures localized inside the wedge and closer to the advancing indenter.

4.2. Geometrical and structural effects of inherited zones of weakness, inferences from analogue modelling and their application for natural laboratories

Strain localization at weak zone(−s) leads to the development of oblique thrust structures in the brittle domain, which link or overlap with structures formed at the weak zones. Other analogue modelling studies addressing the along strike propagation of thrust structures have focused on differences in friction at the base of a thrust wedge (e.g. Calassou et al., 1993; Bahroudi and Koyi, 2003) or the tapering of sedimentary strata at high angle to the convergence direction (eg. Soto et al., 2002). In either case the resulting transfer zones, connecting domains of different material behaviour, is dominantly characterized by oblique thrusts much alike our models with narrow pre-existing weak zones (models 4, 5 and 6, Fig. 3). However, our models show that the obliqueness of thrust structures extents across the entire width of the strong domain, irrespective of the initial distance between the moving wall and the weak zone.

Such types of contractional step-overs are common in natural situations, which served as a base for our modelling design and strategy. For instance, the connection between the Balkanides and the Pontides a swing in geometries is observed in the SW part of the Black Sea (Munteanu et al., 2011). In this example the inherited crustal weak zones are represented by the Histria Depression and Odessa Shelf, formed during the Cretaceous - Middle Eocene extension that have been inverted during the subsequent Late Eocene - Miocene contraction (Dinu et al., 2005). In this natural example, the brittle domain is represented by the Balkanides- Moesian Platform system (Fig. 5a), with the deformation restricted in the close proximity of the indenter, with little if any deformation transferred N-ward (Stuart et al., 2011). Along strike, the transition into the brittle-ductile domain, represented by the Pontides-Western Black Sea shelf, is accommodated by a swing in the Balkanides thrust belt geometry at their connection with the Western Pontides (Fig. 5a). The swing is the result of the far field strain transfer, N-ward intro the Histria Depression and Odessa Shelf, coeval with a reduced amount of shortening recorded in the onshore Balkans when compared with the onshore equivalent (27 and 5 km, respectively, Stuart et al., 2011, Munteanu et al., 2011). Similar to our model type 6 (Fig. 3j) inversion propagates W-ward into the brittle domain as shown by the inversion recorded along the North Dobrogea Orogen (Hippolyte, 2002), even though the weak zone (e.g. Histria Depression, Fig. 5a) reduces its width by reducing the amount of extension affecting the onshore Moesian Platform and North Dobrogea Orogen (Tambrea, 2007; Munteanu et al., 2011).

Another example is the formation of the Makran accretionary prism (Fig. 5b), that started during the Late Cretaceous in response to the large-scale, N-S, convergence between the Eurasian and Arabian plates, e.g. Central Iran/Lut and Afghan blocks (White and Klitgord, 1976; Platt et al., 1985). The prism is one of the largest active in the world, extending more than 1000 km from the Chaman sinistral strike-slip fault in the east to Minab dextral strike-slip fault in the west (Fig. 5b). Along the Minab fault system, the front of the Makran wedge swings as it connects W-ward with the Zagros fold and thrust belt (Fig. 5b). Internally the width of the Makran prism varies along its strike, wider in front of the Afgan block and narrower in front of the Lut block, corresponding with an increased width of the inner Makran unit (Fig. 5b). This structure results in a swinging geometry of the northern border of the Makran prism. The narrowing of the inner Makran unit corresponds with the termination of the Sistan suture zone, a former Neo-Tethys oceanic branch situated between the Afgan and Lut continental blocks closed after Late Cretaceous times (Alavi, 2007; Burg, 2018). We infer that these swings reflect the differences in the lower plate rheology, owing to the inherited crustal geometry and subduction type, in this case oblique with the oceanic crust wider W-ward (Torsvik and Cocks, 2016), with the BD defined by the Lut block and BDD defined by Afgan block, with the transfer zone along the Sistan Ssuture (Fig. 5b).

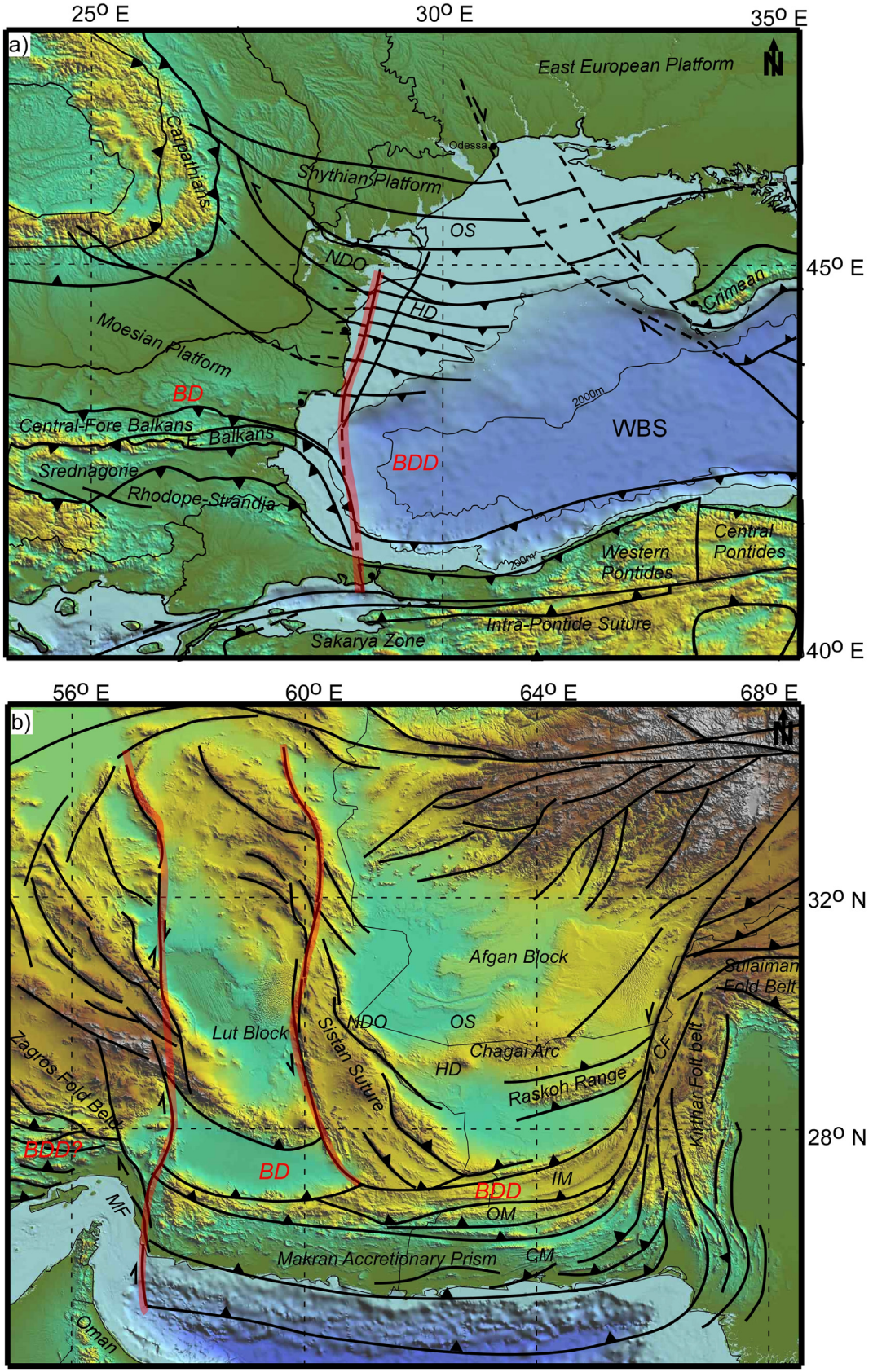

Fig. 5. a) Tectonic sketch of the Western Black Sea Basin and adjacent areas (modified after Munteanu et al., 2011). Note also the far-field transfer of compressional deformation along the Romanian Shelf and the W-ward propagation. HD-Histria Depression, NDO-North Dobrogea Orogen, OS-Odessa Shelf. b) Tectonic sketch of the Makran orogenic wedge and adjacent blocks (redraw after Burg, 2018). Note the transfer zone towards the Zagros fold belt and the swinging geometry of the Sistan Mountain Belt, developed at the contact between Lut and Afgan Block. The inferred limit between BD and BDD is illustrated by the red transparent line. CF- Chaman Fault, MF-Minab Fault; CM-Coastal Makran, IM-inner Makran and OM-Outer Makran. BD- Brittle Domain, BDD- Brittle Ductile. (For interpretation of the references to colour in this figure legend, the reader is referred to the web version of this article.)

Southward the situation looks different with the Oman subduction system being the weak zone, transferring the deformation southward along the subduction front (Fig. 5b). More to the west, we may also speculate that the Zagros fold and thrust belt (Mouthereau et al., 2007) might be the equivalent of our brittle-ductile domain equivalent of our analogue modelling, while the Makran accretion prism should be is the brittle domain, with the transfer zone defined by the Minab fault (Fig. 5b).

One other possible area for the application of our modelling result is the Albanides thin-skinned fold and thrust belt, which displays a typical out-of-sequence and along strike migration of deformation at the junction between the Dinaridic and Hellenic Cenozoic deformation (e.g., Roure et al., 2010; Vilasi et al., 2009). The reason of this step-over can be related to the lateral termination of the Budva - Pindos and Ionian extensional system in the area of the Hellenides (Schmid et al., 2008) and their potentially associated far-field deformation. However, the lack of available details concerning the structure and evolution of this latter area does not allow a detailed comparison with our analogue modelling.

5. Conclusions

Our experimental results show that the presence of crustal weak zones and their associated far-field strain localisation of deformation create a large-scale swinging geometry in orogenic forelands, even if the kinematics of contraction do not change along the orogenic strike. Strain transmission and deformation localization to weak zones with finite orogen-parallel extent, situated in the foreland of mountain belts, leads to the formation of large-scale, transcurrent contractional step-overs, where structures of the different rheological domains connect or overlap. This might be an important observation when analysing short distance changes in thrust belt geometries, particularly when weak zones are not obvious or buried at large depths beneath post-rift sediments. In this case, discriminatory evidences are provided by the out-of-sequence character of deformation in the transfer zone, the swinging geometries in migrating thrusting between domains along their strike and their transcurrent character.

At mantle lithospheric level, our results show that the presence of weak zones in the crust will be reflected in the symmetry and amplitude of lithospheric folding. In weak lithospheric domains (the brittle-ductile domain in our models), symmetric folding will be observed bellow the weak zone, its amplitude being constrained by the amount of localized crustal shortening. In contrast, the dispersion of crustal deformation across multiple weak zones will result in a flatter lithospheric base, with low amplitude folding if any. In strong lithospheric domains, the localized crustal deformation will be accommodated at mantle lithospheric levels by asymmetric folding with the same vergence compare to major thrusts in the crust.

Acknowledgements

The experiments were performed at the Tectonic Modelling Laboratory (TecLab) of Utrecht University, where we benefited from Inge Van Gelder's assistance. Elisa Calignano, Melody Philippon and Endre Dombradi are acknowledged for fruitful suggestions during modelling. This research project was financially supported by Universiteit Utrecht, Netherlands. We are grateful to the comments of the Associated Editor Matthias Rosenau and the comments of Michael Warsitzka, Bertrand Maillot and anonymous reviewers. They have significantly improved the original manuscript.

References

Alavi, M., 2007. Structures of the Zagros fold-thrust belt in Iran. Am. J. Sci. 307, 1064–1095.
Baes, M., Govers, R., Wortel, R., 2011. Switching between alternative responses of the lithosphere to continental collision. Geophys. J. Int. 187, 1151–1174.
Bahroudi, A., Koyi, H.A., 2003. The effect of spatial distribution of Hormuz salt on deformation style in the Zagros fold and thrust belt: an analogue modeling approach. J. Geol. Soc. Lond. 160 (5), 719–733.
Banks, C.I., Robinson, A.G., Williams, M.P., 1997. Structure and Regional Tectonics of the Achara-Trialet Fold Belt and the Adjacent Rioni and Kartli Foreland Basins, Republic of Georgia. In: Robinson, A.G. (Ed.), Tectonic-Sedimentary Evolution of the North-Tethyan Margin in the Central Pontides of Northern Turkey. AAPG, Tulsa, Oklahoma, pp. 313–330.
Brun, J.-P., Nalpas, T., 1996. Graben inversion in nature and experiments. Tectonics 15, 677–687.
Buiter, S.J.H., Pfiffner, O.A., Beaumont, C., 2009. Inversion of extensional sedimentary basins: a numerical evaluation of the localisation of shortening. Earth Planet. Sci. Lett. 288, 492–504.
Burg, J.-P., 2018. Geology of the onshore Makran accretionary wedge: Synthesis and tectonic interpretation. Earth Sci. Rev. 185, 1210–1231.
Burov, E., Cloetingh, S., 2009. Controls of mantle plumes and lithospheric folding on modes of intraplate continental tectonics: differences and similarities. Geophys. J. Int. 178, 1691–1722.
Burov, E., Toussaint, G., 2007. Surface processes and tectonics: forcing of continental subduction and deep processes. Glob. Planet. Chang. 58, 141–164.
Calassou, S., Larroque, C., Malavieille, J., 1993. Transfer zones of deformation in thrust wedges: an experimental study. Tectonophysics 221 (3–4), 325–344.
Calignano, E., Sokoutis, D., Willingshofer, E., Gueydan, F., Cloetingh, S., 2015a. Strain localization at the margins of strong lithospheric domains: Insights from analog models. Tectonics 34, 396–412.
Calignano, E., Sokoutis, D., Willingshofer, E., Gueydan, F., Cloetingh, S., 2015b. Asymmetric vs. symmetric deep lithospheric architecture of intra-plate continental orogens. Earth Planet. Sci. Lett. 424, 38–50.
Calignano, E., Sokoutis, D., Willingshofer, E., Brun, J.P., Gueydan, F., Cloetingh, S., 2017. Oblique contractional reactivation of inherited heterogeneities: Cause for arcuate orogens. Tectonics 36, 542–558.
Cloetingh, S., Spadini, G., Van Wees, J.D., Beekman, F., 2003. Thermo-mechanical modelling of Black Sea Basin (de)formation. Sediment. Geol. 156, 169–184.
Cotton, J.T., Koyi, H.A., 2000. Modeling of thrust fronts above ductile and frictional detachments: Application to structures in the Salt Range and Potwar Plateau, Pakistan. GSA Bull. 112, 351–363.
De Franco, R., Govers, R., Wortel, R., 2008. Nature of the plate contact and subduction zones diversity. Earth Planet. Sci. Lett. 271, 245–253.
Del Ventisette, C., Montanari, D., Sani, F., Bonini, M., 2006. Basin inversion and fault reactivation in laboratory experiments. J. Struct. Geol. 28, 2067–2083.
Dinu, C., Wong, H.K., Tambrea, D., Matenco, L., 2005. Stratigraphic and structural characteristics of the Romanian Black Sea shelf. Tectonophysics 410, 417–435.
Doglioni, C., Carminati, E., Cuffaro, M., Scrocca, D., 2007. Subduction kinematics and dynamic constraints. Earth Sci. Rev. 83, 125–175.
Dombrádi, E., Sokoutis, D., Bada, G., Cloetingh, S., Horváth, F., 2010. Modelling recent deformation of the Pannonian lithosphere: Lithospheric folding and tectonic topography. Tectonophysics 484, 103–118.
Dubois, A., Odonne, F., Massonnat, G., Lebourg, T., Fabre, R., 2002. Analogue modelling of fault reactivation: tectonic inversion and oblique remobilisation of grabens. J. Struct. Geol. 24, 1741–1752.
Erdős, Z., Huismans, R.S., van der Beek, P., Thieulot, C., 2014. Extensional inheritance and surface processes as controlling factors of mountain belt structure. J. Geophys. Res. Solid Earth 119, 9042–9061.
Farzipour-Saein, A., Koyi, H., 2014. Effect of lateral thickness variation of an intermediate decollement on the propagation of deformation front in the Lurestan and Izeh zones of the Zagros fold-thrust belt, insights from analogue modeling. J. Struct. Geol. 65, 17–32.
Graveleau, F., Malavieille, J., Dominguez, S., 2012. Experimental modelling of orogenic wedges: a review. Tectonophysics 538-540, 1–66.
Hatzfeld, D., Authemayou, C., Beek, P.v.d., Bellier, O., Lavé, J., Oveisi, B., Tatar, M., Tavakoli, F., Walpersdorf, A., Yamini-Fard, F., 2010. In: Leturmy, P., Robin, C. (Eds.), The Kinematics of the Zagros Mountains (Iran). Tectonic and Stratigraphic Evolution of Zagros and Makran during the Mesozoic–Cenozoic. Geological Society of London, pp. 0.
Herbert, J.W., Cooke, M.L., Souloumiac, P., Madden, E.H., Mary, B.C., Maillot, B., 2015. The work of fault growth in laboratory sandbox experiments. Earth Planet. Sci. Lett. 432, 95–102.
Hippolyte, J.C., 2002. Geodynamics of Dobrogea (Romania); new constraints on the evolution of the Tornquist-Teisseyre Line, the Black Sea and the Carpathians. Tectonophysics 357, 33–53.
Hubbert, M.K., 1937. Theory of scale models as applied to the study of geologic structures. Geol. Soc. Am. Bull. 48, 1459–1520.
Koyi, H., Sans, M., 2006. Deformation transfer in viscous detachments: Comparison of sandbox models to the South Pyrenean Triangle Zone. In: Buiter, S.J.H., Schreurs, G. (Eds.), Analogue and Numerical Modelling of Crustal-Scale Processes, (Geological).
Lacombe, O., Bellahsen, N., 2016. Thick-skinned tectonics and basement-involved fold–thrust belts: insights from selected Cenozoic orogens. Geol. Mag. 153, 763–810.
Luth, S., Willingshofer, E., Sokoutis, D., Cloetingh, S., 2010. Analogue modelling of continental collision: Influence of plate coupling on mantle lithosphere subduction, crustal deformation and surface topography. Tectonophysics 484, 87–102.
McCall, G.J.H., Kidd, R.G.W., 1982. The Makran, Southeastern Iran: the anatomy of a convergent plate margin active from Cretaceous to present. Geol. Soc. Lond., Spec. Publ. 10 (1), 387.
Michon, L., Sokoutis, D., 2005. Interaction between structural inheritance and extension direction during graben and depocentre formation: an experimental approach.

Tectonophysics 409, 125–146.
Morley, C.K., 1988. Out of sequence thrusts. Tectonics 7 (6), 539–561.
Mouthereau, F., Lacombe, O., Tensi, J., Bellahsen, N., Kargar, S., Amrouch, K., 2007. Mechanical Constraints on the Development of the Zagros Folded Belt (Fars). In: Lacombe, O., Roure, F., Lavé, J., Vergés, J. (Eds.), Thrust Belts and Foreland Basins. Springer Berlin Heidelberg, Berlin, Heidelberg, pp. 247–266.
Munteanu, I., Matenco, L., Dinu, C., Cloetingh, S., 2011. Kinematics of back-arc inversion of the Western Black Sea Basin. Tectonics 30 (5), 21.
Munteanu, I., Willingshofer, E., Sokoutis, D., Matenco, L., Dinu, C., Cloetingh, C., 2013. Transfer of deformation in back-arc basins with a laterally variable rheology: constraints from analogue modelling of the Balkanides - Western Black Sea inversion. Tectonophyiscs 602, 223–236.
Munteanu, I., Willingshofer, E., Matenco, L., Sokoutis, D., Cloetingh, S., 2014. Far-field contractional polarity changes in models and nature. Earth Planet. Sci. Lett. 395, 101–115.
Nalpas, T., Le Douran, S., Brun, J.P., Untrnehr, P., Richert, J.P., 1995. Inversion of the Broad Fourteens Basin (offshore Netherlands), a small-scale model investigation. Sediment. Geol. 95, 237–250.
Nieuwland, D.A., Leutscher, J.H., Gast, J., 2000. Wedge equilibrium in foldand-thrust belts: prediction of out-of-sequence thrusting based on sandbox experiments and natural examples. Geol. Mijnb. 79, 81–91.
Panien, M., Schreurs, G., Pfiffner, A., 2005. Sandbox experiments on basin inversion: testing the influence of basin orientation and basin fill. J. Struct. Geol. 27, 433–445.
Platt, J.P., Leggett, J.K., Young, J., Raza, H., Alam, S., 1985. Large-scale sediment underplating in the Makran accretionary prism, Southwest Pakistan. Geology 13, 507–511.
Ramberg, H., 1981. Gravity, Deformation and the Earth's Crust. Academic Press, London.
Ranalli, G., Murphy, D.C., 1987. Rheological stratification of the lithosphere. Tectonophysics 132, 281–295.
Roure, F., 2008. Foreland and Hinterland basins: what controls their evolution? Swiss J. Geosci. 101, 5–29.
Roure, F., Cloetingh, S., Scheck-Wenderoth, M., Ziegler, P.A., 2010. Achievements and challenges in Sedimentary Basin Dynamics: A Review. In: Cloetingh, S., Negendank, J. (Eds.), New Frontiers in Integrated Solid Earth Sciences. Springer, Netherlands, pp. 145–233.
Sadeghi, S., Storti, F., Yassaghi, A., Nestola, Y., Cavozzi, C., 2016. Experimental deformation partitioning in obliquely converging orogens with lateral variations of basal décollement rheology: Inferences for NW Zagros, Iran. Tectonophysics 693, 223–238.
Schmid, S.M., Bernoulli, D., Fügenschuh, B., Matenco, L., Schefer, S., Schuster, R., Tischler, M., Ustaszewski, K., 2008. The Alpine-Carpathian-Dinaridic orogenic system: correlation and evolution of tectonic units. Swiss J. Geosci. 101, 139–183.
Smit, J.H.W., Brun, J.P., Sokoutis, D., 2003. Deformation of brittle-ductile thrust wedges in experiments and nature. J. Geophys. Res. 108, 2480.
Sokoutis, D., Willingshofer, E., 2011. Decoupling during continental collision and intraplate deformation. Earth Planet. Sci. Lett. 305, 435–444.
Sokoutis, D., Bonini, M., Medvedev, S., Boccaletti, M., Talbot, C.J., Koyi, H., 2000. Indentation of a continent with a built-in thickness change: experiment and nature. Tectonophysics 320, 243–270.
Sokoutis, D., Burg, J.-P., Bonini, M., Corti, G., Cloetingh, S., 2005. Lithospheric-scale structures from the perspective of analogue continental collision. Tectonophysics 406, 1–15.
Soto, R., Casas, A.M., Storti, F., Faccenna, C., 2002. Role of lateral thickness variations on the development of oblique structures at the western end of the South Pyrenean Central Unit. Tectonophysics 350 (3), 215–235.
Stuart, C.J., Nemcok, M., Vangelov, D., Higgins, E.R., Welker, C., Meaux, D.P., 2011. Structural and depositional evolution of the East Balkan thrust belt, Bulgaria. AAPG Bull. 95, 649–673.
Tambrea, D., 2007. Subsidence Analysis and Thermo-Tectonic Evolution of Histria Depresion (Black Sea). Implications in Hydrocarbon Generation. Faculty of Geology and Geophysics. University of Bucharest, Bucharest, pp. 165.
Tarapoanca, M., 2004. Architecture, 3D Geometry and Tectonic Evolution of the Carpathians Foreland Basin. Faculty of Earth and Life Sciences. VU University Amsterdam, Amsterdam, pp. 120.
Tesauro, M., Kaban, M.K., Cloetingh, S.A.P.L., 2012. Global strength and elastic thickness of the lithosphere. Glob. Planet. Chang. 90–91, 51–57.
Torsvik, T.H., Cocks, L.R.M., 2016. Earth History and Palaeogeography. Cambridge University Press, Cambridge, pp. 317.
Vilasi, N., Malandain, J., Barrier, L., Callot, J.-P., Amrouch, K., Guilhaumou, N., Lacombe, O., Muska, K., Roure, F., Swennen, R., 2009. From outcrop and petrographic studies to basin-scale fluid flow modelling: the use of the Albanian natural laboratory for carbonate reservoir characterisation. Tectonophysics 474, 367–392.
Vogt, K., Matenco, L., Cloetingh, S., 2017. Crustal mechanics control the geometry of mountain belts. Insights from numerical modelling. Earth Planet. Sci. Lett. 460, 12–21.
Watts, A.B., 2001. Isostasy and Flexure of the Lithosphere. Cambridge University Press, Cambridge, pp. 455.
Weijermars, R., Schmeling, H., 1986. Scaling of Newtonian and non-Newtonian fluid dynamics without inertia for quantitative modelling of rock flow due to gravity (including the concept of rheological similarity). Phys. Earth Planet. Inter. 43, 316–330.
White, R.S., Klitgord, K., 1976. Sediment deformation and plate tectonics in the Gulf of Oman. Earth Planet. Sci. Lett. 32, 199–209.
Willingshofer, E., Sokoutis, D., 2009. Decoupling along plate boundaries: Key variable controlling the mode of deformation and the geometry of collisional mountain belts. Geology 37, 39–42.
Willingshofer, E., Sokoutis, D., Burg, J.-P., 2005. Lithospheric-scale analogue modelling of collision zones with a pre-existing weak zone. In: Gapais, D., Brun, J.P., Cobbold, P.R. (Eds.), Deformation Mechanisms, Rheology and Tectonics: From Minerals to the Lithosphere. vol. Volume 243. Geol. Soc. London, Spec. Publ, pp. 277–294.
Willingshofer, E., Sokoutis, D., Luth, S.W., Beekman, F., Cloetingh, S., 2013. Subduction and deformation of the continental lithosphere in response to plate and crust-mantle coupling. Geology 41, 1239–1242.
Willingshofer, Ernst; Sokoutis, Dimitrios; Beekman, Fred; Schönebeck, Jan-Michael; Warsitzka, Michael; Rosenau, Matthias (2018): Ring Shear Test Data of Feldspar Sand and Quartz Sand Used in the Tectonic Laboratory (TecLab) at Utrecht University for Experimental Earth Science Applications. vol. V. 1. GFZ Data Services. doi:https://doi.org/10.5880/fidgeo.2018.072.
Ziegler, P.A., van Wees, J.-D., Cloetingh, S., 1998. Mechanical controls on collision-related compressional intraplate deformation. Tectonophysics 300, 103–129.
Ziegler, P.A., Bertotti, G., Cloetingh, S., 2002. Dynamic processes controlling foreland development - the role of mechanical (de)coupling of orogenic wedges and forelands. In: Bertotti, G., Schulmann, K., Cloetingh, C. (Eds.), Continental Collision and the Tectono-Sedimentary Evolution of Forelands, pp. 17–56.